UCLA
UCLA Electronic Theses and Dissertations

Title
Modeling of Electronic Cell-Substrate Impedance Sensing for Single Cell

Permalink
https://escholarship.org/uc/item/2075c8f0

Author
Ren, Dingkun

Publication Date
2013

Peer reviewed|Thesis/dissertation

eScholarship.org Powered by the California Digital Library
University of California

UNIVERSITY OF CALIFORNIA

Los Angeles

Modeling of Electronic Cell-Substrate Impedance Sensing for Single Cell

A thesis submitted in partial satisfaction

of the requirements for the degree Master of Science

in Electrical Engineering

by

Dingkun Ren

2013

© Copyright by

Dingkun Ren

2013

ABSTRACT OF THE THESIS

Modeling of Electronic Cell-Substrate

Impedance Sensing for Single Cell

by

Dingkun Ren

Master of Science in Electrical Engineering

University of California, Los Angeles, 2013

Professor Chi On Chui, Chair

The thesis studies a three-dimensional rectangular hexahedron meshing (3D RHM) single-cell model to explore the cell behaviors for electronic cell-substrate impedance sensing (ECIS). In the model, a spatial network of resistors (R) and capacitors (C) is established to mimic a single-cell measurement system including electrodes, medium and mammalian cells. Unlike the existing ECIS models, which are limited by several approximations for current flow, spreading resistance and cell morphology, the proposed single-cell model is more flexible and enables us to provide high mesh resolution to reconstruct the real circumstances of cell and their surroundings. Moreover, the simulated results by single-cell model match the published measurement and simulation data by Thein and Huang. In addition, it is also demonstrated that

the maximum change of total impedance (Z) between 100 Hz to 10 MHz varies based upon changes in cell properties, specifically the size of cell, cell membrane capacitance, cell-electrode distance, and cytoplasm resistivity, which is essential to understand the frequency-dependent cell behaviors.

The thesis of Dingkun Ren is approved.

Wentai Liu

Yuanxun Wang

Chi On Chui, Committee Chair

University of California, Los Angeles

2013

Table of Contents

List of Acronyms

1D	One-dimensional
2D	Two-dimensional
3D	Three-dimensional
A	Area
Au	Gold
C	Capacitor
Cr	Chromium
CTL	Cartesian transport lattice
CTX	Chlorotoxin
ECIS	Electronic cell-substrate impedance sensing
EM	Electromagnetics
FEM	Finite element method
FDTD	Finite-difference time-domain
IHP	Inner Helmholtz plane
KRGD	Lysine–arginine–glycine–aspartic acid
L	Distance
NIH3T3	Mouse fibroblast cell
OHP	Outer Helmholtz plane
RHM	Rectangular hexahedron meshing
R	Resistor
RMS	Root mean square
SAM	Self-assembled monolayer

U87MG	Human glioblastoma cell
Z	Impedance

List of Symbols

A	Area between two mesh nodes
A_n	Effective area between two mesh nodes
β	Phase constant for Warburg impedance at electro/electrolyte interface
C_{CPE}	Specific capacitance for Warburg impedance at electro/electrolyte interface
C_d	Specific capacitance of double-layer
C_m	Specific capacitance of cell membrane
C_{spec}	Specific capacitance
$C_{W,n}$	Capacitance of Warburg impedance between two mesh nodes
d	Cell-electrode distance
D	Diameter of working electrode
D_{cell}	Diameter of cell
ε	Dielectric constant
f	Frequency of input sinusoidal signal
$j\omega t$	Phase term of sinusoidal signal
k	Constant for Warburg impedance in Huang's model
L	Distance between two mesh nodes
L_n	Effective distance between two mesh nodes
φ	Extra phase term of sinusoidal signal
ρ_S	Resistivity of solution
R_{ct}	Charge transfer resistance in double-layer
$R_{Cyto,n}$	Resistance of cytoplasm between two mesh nodes
R_{limit}	Limiting resistance

R_s	Spreading resistance
$R_{S,n}$	Resistance of solution between two mesh nodes
R_{spec}	Specific resistance
$R_{W,n}$	Resistance of Warburg impedance between two mesh nodes
V_0	Amplitude of sinusoidal signal from source meter
V_{cell}	Output sinusoidal signal between electrodes with cells
V_{in}	Amplitude of input sinusoidal signal for HPSICE simulation
V_{nocell}	Output sinusoidal signal between electrodes without cells
V_{souce}	Sinusoidal signal from source meter
ΔZ	Difference between total impedance between electrodes with and without cells
Z_{cell}	Total impedance between electrodes with cells
$Z_{Interface,n}$	Electrode/electrolyte impedance between two mesh nodes
$Z_{Membrane,n}$	Impedance of cell membrane between two mesh nodes
Z_{nocell}	Total impedance between electrodes without cells
$Z_{normalized}$	Normalized impedance
$Z_{W,n}$	Warburg impedance between two mesh nodes

Chapter 1

Introduction

Electronic cell-substrate impedance sensing (ECIS) is a real-time, non-invasive and label-free electrical monitor technique for cell and tissue behavior in vitro [1]. It was firstly published in 1984 by I. Giaever and C. R. Keese from General Electric Research Laboratory [2]. The cellular behaviors that can be detected by ECIS measuring system include, but not limited to 1) cell adhesion, 2) micromotion, 3) mitosis, 4) spreading, and 5) response to the drugs. Therefore, ECIS has been largely used in the living cell monitor to understand cell motility, cell membrane, cytoplasm, organelles and toxicity of drugs. In the past three decades, an incredible growth in the field of ECIS has not only resulted in a large amount of academic research but also biological companies such as Applied Biophysics and ACEA Biosciences [3, 4], where different types of microelectrodes have been designed and fabricated to monitor various types of cells.

1.1 Measurement System of ECIS

In ECIS measurement system illustrated in Fig. 1 [5], biological cells attach to a small gold microelectrode called working electrode, where another gold electrode serves as the counter electrode with much larger size. Electrodes are seated inside a well, which is fulfilled with medium, i.e. electrolyte, and provides the necessary living circumstance for cells. Before cells are inoculated onto the electrode, the total impedance of system is only affected by the double layer at electrode/medium interface and the large amount of medium in the well. When cells

spread on the working electrode, the distribution of current flow will change due to high resistance of cell membrane which is composed of two layers of lipid.

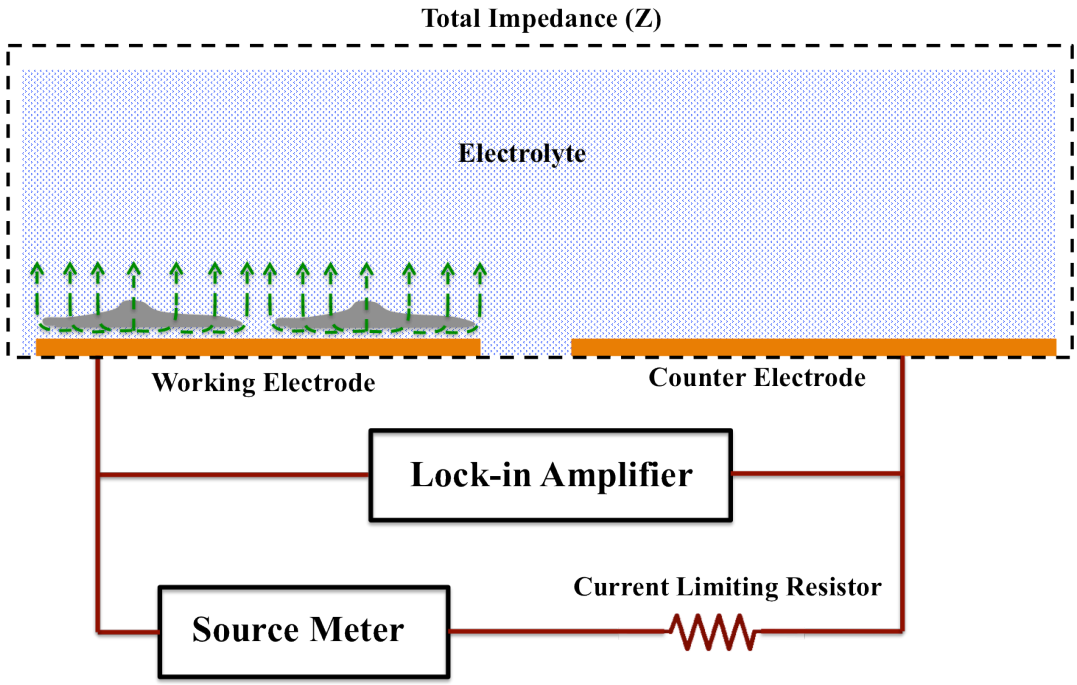

Figure 1 ECIS measurement system. The green dash curves present the distribution of current flow. The size of electrodes, cells and peripheral circuits are not to scale.

During the measurement, a sinusoidal voltage signal at a certain frequency f is generated by source meter and applied on two electrodes through a high current limiting resistor R_{limit}. Thus, the voltage across the lock-in amplifier can be described as:

$$V_{nocell} = \frac{Z_{nocell}}{R_{\lim it} + Z_{nocell}} V_{source} \tag{1}$$

$$V_{cell} = \frac{Z_{cell}}{R_{\lim it} + Z_{cell}} V_{source} \tag{2}$$

where $V_{source} = V_0 e^{j\omega t}$; V_{nocell} and V_{cell} represent the voltages on two electrodes without and with cells, respectively.

Since Z_{nocell} and Z_{cell} are both complex numbers, Eqn. (1) and (2) can be further written as [6]:

$$V_{nocell} = |V_{nocell}| e^{j(\omega t + \varphi_1)} \tag{3}$$

$$V_{cell} = |V_{cell}| e^{j(\omega t + \varphi_2)} \tag{4}$$

Finally, the amplitude and the phase are eventually detected by the lock-in amplifier and the actual values of impedance in two cases are calculated.

From Eqn. (1) and (2), the difference of total impedance without and with cells is calculated as:

$$\Delta Z = Z_{cell} - Z_{nocell} \tag{5}$$

Since the total impedance is a complex number, it varies with frequency. The sensitivity of ECIS measurement system can be defined as the normalized impedance, which is written as:

$$Z_{normalized} = \frac{\Delta Z}{Z_{nocell}} = \frac{Z_{cell} - Z_{nocell}}{Z_{nocell}} \tag{6}$$

The larger $Z_{normalized}$ is, the higher sensitivity can be obtained by the measurement. Since the cell membrane is mainly composed of a lipid bilayer of phospholipid molecules [7], it is highly insulated and can be considered as a capacitor. When cells adhere on the electrode, it can be assumed that several insulating disks start to contact closely with the electrode to block the current flow. Therefore, the current has to pass the limited space between the bottom of cell and the electrode, where the resistance of medium underneath the cell is large due to a small separation in the vertical direction.

1.2 Applications and Products of ECIS

Cell utilized in ECIS measurement should be adhesive to seat on electrode as shown in Fig. 2. After cells are introduced onto the electrode, they start to spread across the substrate. The whole spreading procedure takes about 24 hours and then cells are ready to be measured [5, 8].

While cells are alive, they will keep moving on the substrate and be affected by their circumstances; therefore, such cellular behaviors eventually contribute to the change of the total impedance.

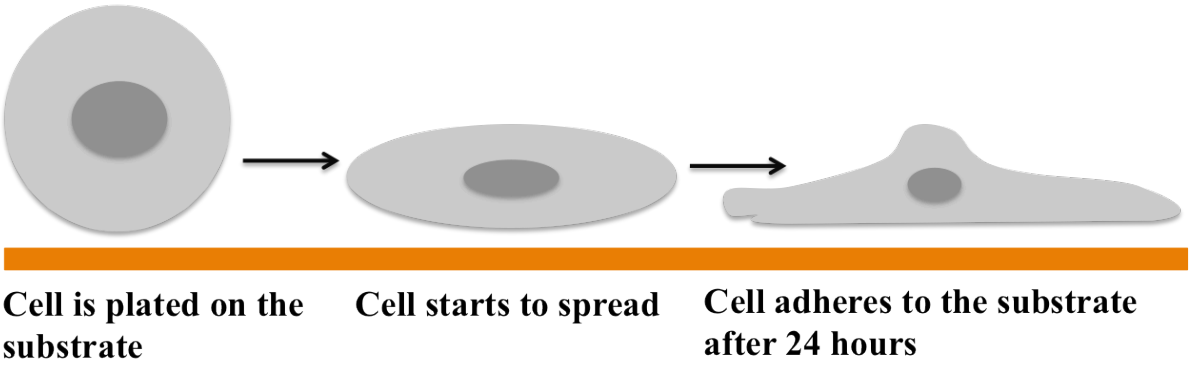

Figure 2 The preparation of cells for ECIS measurement.

Several cell behaviors detected by ECIS measurement system are listed below with published research studies:

I. Adhesion of cell

Adhesion of cell is significant in ECIS measurement since non-adhesive cell is impossible to be measured by electrode substrate. Therefore, many works have been done to explore the effects of different peptides for electrode surface modification to improve the cell adhesion.

Giaever and Keese utilized four different protein, bovine serum albumin, gelatin, bovine fetuin, and human plasma fibronectin, to test the adhesion for both WI-38 and cancer cell WI-38 VA 13 [8]. Lysine–arginine–glycine–aspartic acid (KRGD) and fibronectin were also used to form covalent bonds on gold electrode to examine the adhesion of mouse fibroblast cells (NIH3T3) [5]. Last but not least, ECIS sensing chip was used to monitor the self-assembled monolayer (SAM) formed by various concentration of cysteine [6].

II. *Spreading of cell*

The mechanism of cell spreading is similar with cell adhesion because large spreading relies on the strong adhesion on electrode, which is coated with specific protein. As shown in Fig. 2, the spreading of cell leads to a larger coverage of area and thus the total impedance will be increased. In Giaever and Keese's work, both WI-38 cells and transformed cancer cells WI-38 VA13 were inoculated on the separated electrodes and the changes of voltage in millivolt detected by lock-in amplifier was observed along a period of 48 hours [2]. Similarly, two types of peptides, fibronectin and polyL-lysine, were used to modify microelectrode to increase the spreading of NIH3T3 cells and they were measured for 25 hours to compare the attachment between cells [9].

III. Response to drug treatment

Drug treatment is the most important application of ECIS for cell and tissue. The response of a single cell or tissue to a specific drug in ECIS measurement may be reflected to the change of cell morphology, cell volume, the detachment from substrate or even the death of cell. Through the variance of cell properties after drug treatment, the mechanism of reaction between cells and drugs can be decoded to understand cell cytotoxicity and related pathology. In Qiu's experiment, tumor necrosis factor-α was injected into petri dish to react with cardiomyocytes on Cr/Au electrode and the decrease of impedance was observed. The reason was explained that the average cell-substrate distance was increased due to non-adhesive property of dead cells [10]. Interestingly, drug response in single-cell level was also explored in Asphahani's work where the size of human glioblastoma (U87MG) cells were shrunk after chlorotoxin (CTX) treatment [11].

In this study, CTX in different concentrations were used to identify the cell response and the results were recorded as the normalized impedance versus time.

IV. *Products of ECIS measurement system*

Two ECISs companies are introduced in this subsection.

Applied Biophysics was founded by the pioneers in the field of ECIS – two of them were I. Giaever and and C. R. Keese [3]. Different kinds of array for cell assay were provided by the company, such as the array station with 16 wells and 96 wells as shown in Fig. 3. Each well contains different types of electrodes – single electrode and multielectrode electrode. Moreover, each kind of electrode is recommended to use for certain applications such as cell attachment, cell differentiation, cytotoxicity and cell migration [3].

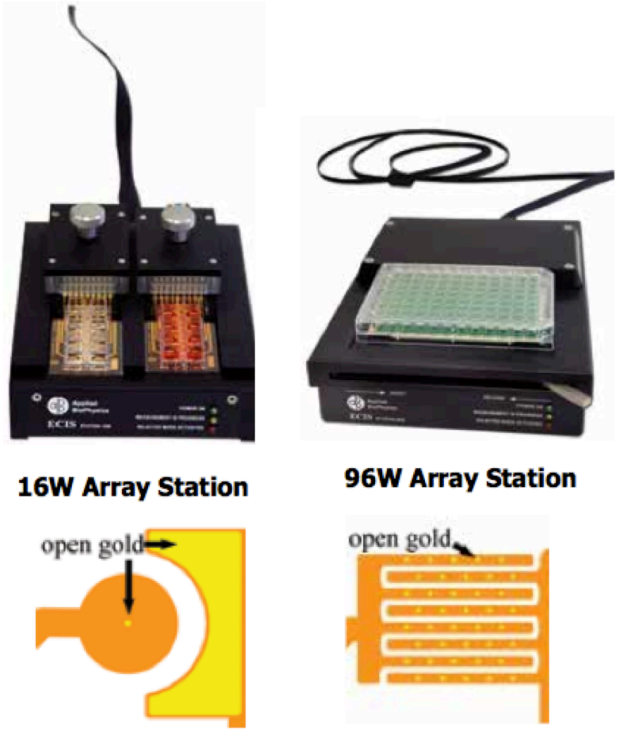

Figure 3 Selected products at Applied Biophysics. The upper two products are the array stations. The bottom two drawings presents the design of single electrode and multielectrode, respectively [3].

ACEA Biosciences, established in 2002, also supports ECIS solution and techniques for various cell assay requirements. Such techniques are allowed to record the cell behavior in real time by providing wireless connection and user interface software. One of the products called iCELLigence is shown in Fig. 4 [4].

Figure 4 The cell assay system iCELLigence from ACEA Biosciences. Such station can be used to record cell growth, proliferation, cytotoxicity, adhesion and morphological dynamics [6].

Even though two companies share the similar idea to examine the cell behaviors, the designs of electrodes and the monitoring indicators are different. First, the geometry of both working electrode and counter electrode is much more complicated in ACEA Biosciences's design with interdigitated shape, while Applied Biophysics uses simple plate electrodes. Second, an indicator called cell index, which is the normalized total impedance sampled at several distinct frequencies, is utilized by ACEA Biosciences to map and categorize the cell properties. In contrast, Applied Biophysics prefers to observe the resistance component, capacitance component, and the normalized total impedance through whole range of measuring frequency.

1.3 Significance of Three-dimensional Model for Single Cell

In the past three decades, ECIS has greatly expanded to biological research for tissue and single cell. However, a key problem that prevents ECIS measurement from being more precise is the lack of a high-performance and easy-operable three-dimensional spatial cell model. Even

though some trails have been made to model cell and tissue with equivalent circuit lumped elements – resistors (R) and capacitors (C), they are either in one-dimensional or two-dimensional, or too coarse to fully reconstruct the morphology of cell. The shape of cell allowed in most of existing models is either circular or rectangular, which restricts to mimic a more complex mammalian cell. Moreover, it is not allowed to produce organelles in those models. Thus, the thesis proposes a three-dimensional rectangular hexahedron meshing (3D RHM) single-cell model to compensate such missing component and provide researchers a high-reproducible modeling approach for further studies.

1.4 Thesis Outline

A literature review for current ECIS modeling approaches is given in Chapter 2, where published models for confluent cell layer and single cell are discussed in details. Moreover, a three-dimensional (3D) Cartesian transport lattice (CTL) model by J. Weaver focusing on cell electroporation and transmembrane voltage is also presented, which serves as an important reference for the development of single-cell model in the thesis.

The methodology of proposed 3D RHM single-cell model is described in Chapter 3. The process of model development is shown with rigorous discussion of boundary conditions and assumptions. Moreover, related simulation software – Gmsh 2.7, MATLAB and Synopsys HSPICE – are also introduced to help readers to replicate the work if interested.

In Chapter 4, the validation of 3D RHM single-cell model is shown by comparing with the measurement and simulation results by Thein and Huang, respectively [2, 12]. Most importantly, the single-cell model is used to analyze the frequency-dependent cell behaviors. It will be presented that the change of total impedance coming from the various cell characteristics

can be projected into different region on frequency spectrum, which is a potential mapping guide for ECIS measurement.

Finally, the whole thesis work is summarized in Chapter 5 and the suggestions for further modeling and measuring work are also recommended.

Chapter 2

Literature Review

In this section, the modeling approaches for ECIS will be discussed based on the theoretical work published in books and articles. The basic idea to reconstruct the electrodes, electrolytes and cells is to utilize lumped element model of circuits. In most of cases, the electrical elements in ECIS models are considered as the passive units, meaning that only resistors (R) and capacitors (C) are used without any active sources.

2.1 Model of Electrode/Medium Interface

In electrochemistry, the interface of electrode and medium is understood as a double-layer region as shown in Fig. 5, where two processes occur simultaneously - faradaic process and nonfaradaic process [13]. In the first process, current is contributed by the charge transfer from the surface to the outer Helmholtz plane (OHP) since the absorption of ions close to the surface of electrode results in the density difference. In contrast, nonfaradaic process results from the electrostatic layer of specific absorbed cations or anions and a virtual capacitance is formed. Therefore, the equivalent circuit model can be simulated as a double-layer capacitor from nonfaradaic process in parallel with the impedance from faradaic process, as shown in Fig. 6 [13]. Moreover, the faradaic impedance can be further modeled as a charge transfer resistor plus Warburg impedance for mass transfer in diffusion layer, and the latter component is considered to be proportional to f^x, where f stands for frequency and x is between 0 and 1 [13]. If the charge

transfer is effective, the resistor R_{ct} can be neglected. Consequently, the total impedance for electrode/medium interface is a frequency-dependent component.

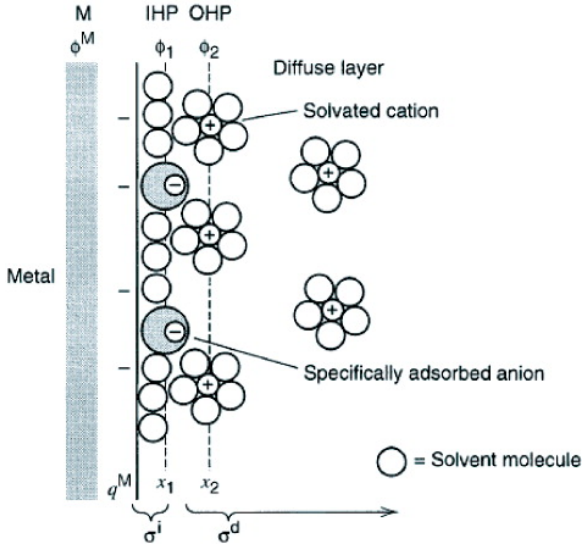

Figure 5 Double layer model of electrode/electrolyte interface. IHP stands for inner Helmholtz plane and OHP is for outer Helmholtz plane [13].

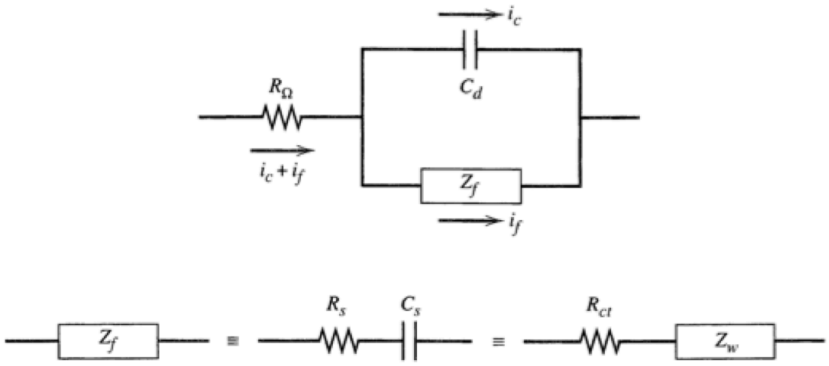

Figure 6 Equivalent circuit model of double layer. C_d is double-layer capacitance and Z_f is faradaic impedance composed of faradaic resistance R_{ct} and Warburg impedance Z_W. [13].

Except the model shown above, the impedance for the whole interface can be also recognized as a constant phase element parallel with the charge transfer resistor R_{ct} [5, 14]. As a result, the impedance of electrode is written as

$$Z_{CPE} = (1/R_{ct} + (j2\pi f)^{\beta} C_{CPE})^{-1} \tag{7}$$

where f is the frequency, β is a constant between 0 and 1, and C_{CPE} is the capacitance.

2.2 Model of Cell

In most of modeling work, the reconstruction of cell is largely simplified where only cytoplasm and cell membrane are considered while organelles are neglected. Cytoplasm can be considered as 'bulk solution' with constant resistivity. Since cell membrane contains an insulating lipid bilayer and protein macromolecules as channel to maintain the transmembrane voltage due to K^+ and Na^+ ions, it can be modeled as a capacitor with several active current sources, shown in Fig. 7 [15].

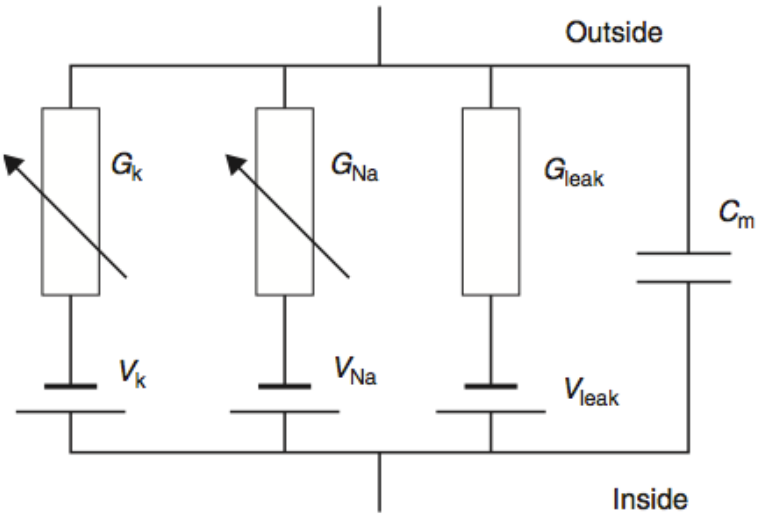

Figure 7 Model of cell membrane. C_m mimics the lipid bilayer, which is highly insulating. G_k, G_{Na} and G_{leak} represent the conductivity of channel protein for passages of ion K^+, ion Na^+ and leakage, while V_K, V_{Na} and V_{leak} are the corresponding transmembrane voltages [15].

In most cases, the membrane model can be further simplified as a passive component – only C_m is considered with the specific capacitance about 1μF/cm^2. Additionally, cell membrane can be measured in different approaches, for instance: 1) it can be subtracted from the cell and put onto an electrode [16]; 2) or electrodes with sharp-end are inserted into cell to contact with two side of membrane [17].

For the morphology of cell, it is mostly simplified as cylindrical or hemi-spherical for the consideration of symmetry, which can help to largely reduce the efforts for calculation. The details of the morphology will be discussed in the section 2.4.

2.3 Model of Medium

Medium surrounding the cell is the bulk medium to support the necessary nutrients and living circumstance. Generally, it is modeled as a spreading resistance because the size of the medium is much larger than the electrode. If the geometry of electrode is a circle with the diameter D, the spreading resistance can be calculated as

$$R_{Spreading} = \frac{\rho}{2D} \tag{8}$$

where ρ is the resistivity of medium.

2.4 Model of Confluent Cell Layer by Giaever and Keese

The pioneering work for ECIS model was done by I. Giaever and C. R. Keese published in 1991 to study the micromotion of cell on electrode [18]. They modeled a confluent VA13 cell layer as many tightly connected cylindrical disks and solved a two-order modified Bessel function. As illustrated in Fig. 8, the cells are plated on a small electrode around 10^{-3} cm^2 and form a single thin layer [18]. In the model, several assumptions are made: 1) the current flow underneath each cell is considered to radiate from the center to the cell edge; 2) the potential above the cell is a constant V_m; 3) cell membrane is simplified as the component with capacitance only. To establish the differential equation, the space between the bottom of cell and the electrode can be separated into infinite small 'rings' with inner radius r and outer radius $r+dr$. In this region, the lateral current flows from the inside of ring to the outside and contributes to

the voltage change dV, while the vertical current moves from the electrode and penetrates through the whole cell. The final modified Bessel function yields

$$\frac{d^2V}{dr^2}+\frac{1}{r}\frac{dV}{dr}-\gamma^2V+\beta=0 \tag{9}$$

and

$$\gamma^2=\frac{\rho}{h}\left(\frac{1}{Z_n}+\frac{1}{Z_m}\right) \tag{10}$$

$$\beta=\frac{\rho}{h}\left(\frac{V_n}{Z_n}+\frac{V_m}{Z_m}\right) \tag{11}$$

where r is the distance from the center of cylindrical cell to the infinite ring element; ρ is the resistivity of medium; h is the distance between the bottle of cell and electrode; Z_n is the impedance of electrode/electrolyte interface; Z_m is the membrane impedance; and V_n and V_m mean the constant potentials of electrode and the outer cell, respectively [18].

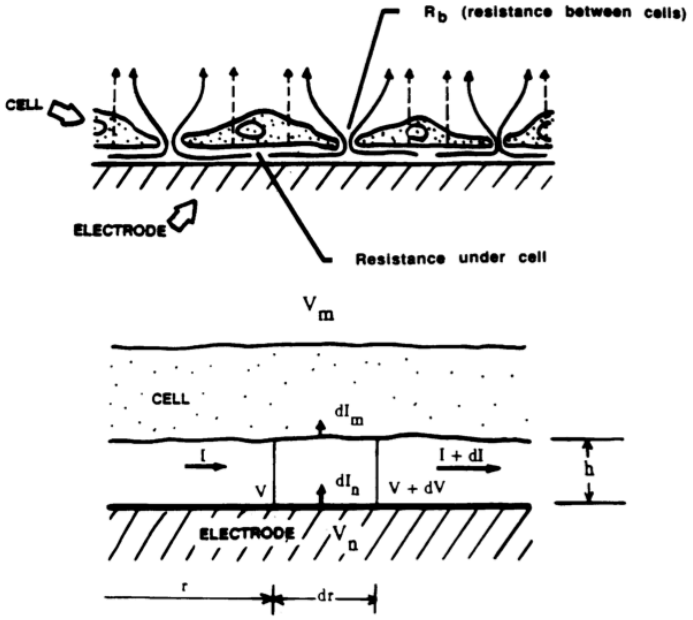

Figure 8 Modeling of confluent cell layer by Giaever and Keese. Cells are closely plated on the electrode with a single layer, where the junction, i.e. a small passage, between two cells is considered as junction resistance R_b. The space between the bottom membrane and the electrode is divided into an infinite small stripe [18].

Two boundary conditions for such Bessel function are [18]

$$I(r=0)=0 \tag{12}$$

$$V(r=r_c)=I(r=r_c)\cdot R_b \tag{13}$$

where r_c is the radius of the cylindrical cell and R_b is the junction resistance between two neighboring cells.

Plugging the boundary conditions into the standard solution for Bessel function, the total impedance can be solved as [18]

$$\frac{1}{Z_c}=\frac{1}{Z_n}\left(\frac{Z_n}{Z_n+Z_m}+\frac{\frac{Z_m}{Z_n+Z_m}}{\frac{\gamma r_c}{2}\frac{I_0(\gamma r_c)}{I_1(\gamma r_c)}+R_b\left(\frac{1}{Z_n}+\frac{1}{Z_m}\right)}\right) \tag{14}$$

where Z_c is the total impedance.

Since Z_n and Z_m are the specific impedance with dimension Ω cm^2, the final result Z_c is also the specific impedance of the confluent cell layer, which needs to be divided by the area of electrode.

It can be seen form Eqn. 14 that the total impedance only depends on two parameters: R_b and h. After data fitting to the measured impedance, R_b and h can be obtained. R_b is a significant indicator to understand the ion flow around the cell, while h is used to explore the cell adhesion, cell attachment, cytotoxicity and so on.

2.5 Model of Single Cell by Huang

In Huang's work, a single cell is modeled by COMSOL Multiphysics using finite element method (FEM) shown in Fig. 9, to understand the current distribution versus the change of input signal frequency and the variance of total impedance due to the change of distance between cell

bottom membrane and electrode [12]. For the consideration of mesh resolution and computation time, several modifications are made for the single cell model: 1) only a quarter of system including cell, electrode and medium is constructed; 2) total space for electrode/electrolyte double layer and membrane/electrode separation is extended into 0.5 μm in vertical direction and the electrical parameters for this region are linearly changed accordingly; 3) the thickness of cell membrane is set as 0.5 μm, fulfilled with the solution.

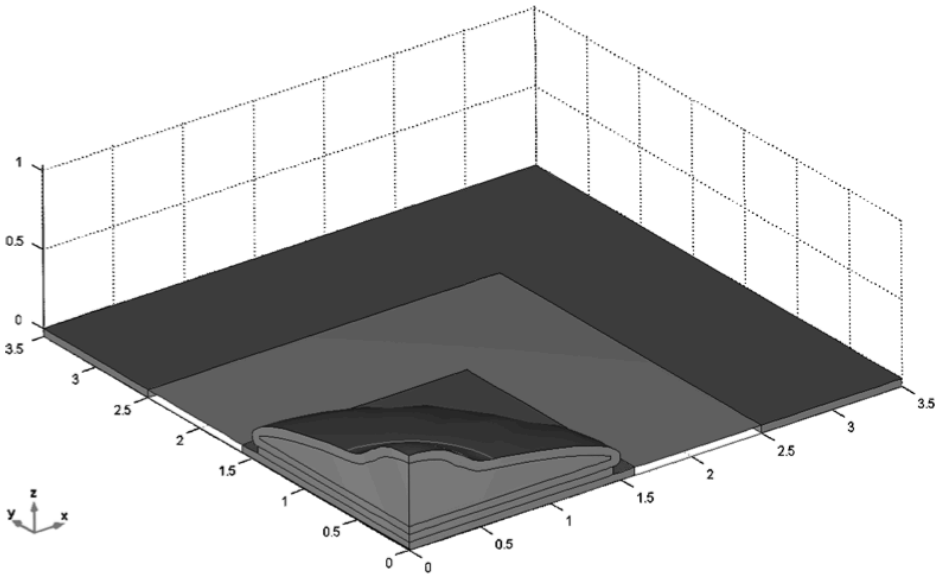

Figure 9 Modeling of single cell by Huang with COMSOL Multiphysics. Only a quarter of system is established to save the computation time. The dark regions show the working electrode and counterelectrode [3].

With the assistance from commercial software, distribution of current flow, potential mapping, and total impedance are easy to be simulated.

2.6 Model of Single Cell by Thein

Another approach to reconstruct a single cell was published by Thein [5]. Similar with Giaever and Keese's work, the space underneath the cell is divided into several sub-regions and each region is connected with equivalent lumped electrical elements, shown in Fig. 10 [5]. In this case, cell membrane is considered as a resistor in parallel with a resistor. By fitting the

measurement data, several parameters are estimated: 1) cell membrane resistivity ρ_m; 2) cell membrane capacitance C_m; 3) cell-electrode distance d.

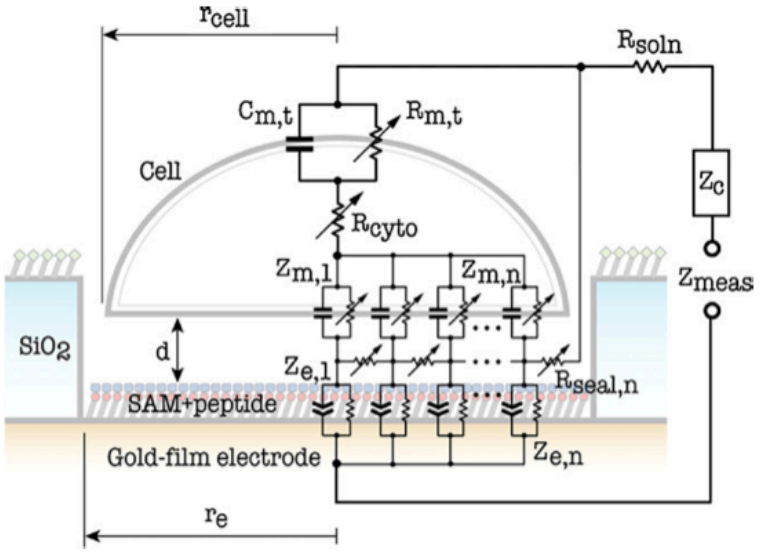

Figure 10 Modeling of single cell by Thein. The total impedance is composed of equivalent lumped electrical elements. The cell is in a hemispherical shape [5].

In this model, several assumptions are made: 1) total cytoplasm is a single resistor; 2) top cell membrane is modeled as a single component with a resistor and a capacitor; 3) the cell size is the same as the electrode; 4) the direction of current flow radiates from the center of electrode. In order to reduce the fitting effort, the number of division, n, is selected as 5. Such model is applied to explore the effect of distance d to the total impedance and drug treatment.

2.7 Model of Single Cell by Weaver

The modeling method designed by Weaver is called Cartesian transport lattice (CTL), where the whole region for simulation is evenly divided into small cubes with the same length and every two nodes on cubes are connected with an impedance component [19]. The value of such component is determined by its location in the system: 1) if it is projected in the area inside or outside the cell, the impedance is replaced by two parallel resistor and capacitor with

corresponding parameters; 2) when the component overlaps with the location of cell membrane, it is considered as a combination of outer electrolyte, membrane and inner cytoplasm which are connected in series, shown in Fig. 11 [19].

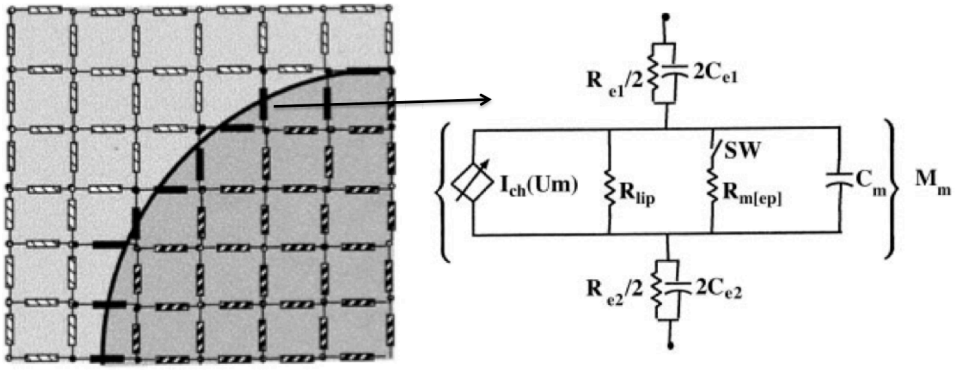

Figure 11 Modeling of single cell by Weaver. The total region is separated by three-dimensional Cartesian transport lattice to be many small cubes composed of impedance elements. The element which can projected into the location of membrane is modeled as a combination of outer electrolyte, membrane and inner cytoplasm which are connected in series [19].

In Weaver's model for cell membrane, four elements are included: 1) membrane capacitance; 2) membrane resistance; 3) active source for ion channel; 4) switch for electroporation.

In the simulation, a spherical cell is put in the middle of a large cubic medium and two sides of bulk cubic are set with voltage boundary conditions to generate an electric field across the cubic. Eventually, a 3D impedance network is established and solved by SPICE and mapping of electrical potential is plotted by MATLAB for cell electroporation. However, similar method has not been used in ECIS research.

2.8 Summary of Different Models and Proposed Model in Thesis

Table 1 summarizes the cell properties focused by each model. Different models cover various cell characteristics which are determined by the specific applications and research goals from different groups. It should be mentioned that 3D CTL model created by Weaver is not for

the application of ECIS, and he utilized the model to understand the electroporation in cells and tissues under high frequency voltage pulses [19-21].

Table 1 SUMMARY OF DIFFERENT MODELS AND PROPOSED MODEL

Cell Properties	Giaever & Keese [2, 8, 18, 22]	Huang [12, 23]	Thein [5, 24-25]	Weaver [19-21]	This Work
Cell-electrode distance d	✔	✔	✔		✔
Cell membrane capacitance C_m	✔				✔
Cell spreading (cell size)	✔	✔	✔		✔
Junction resistance between cells R_b	✔				
Electroporation (transmembrane potential V_m)				✔	
Cytoplasm resistivity ρ_{Cyto}					✔

Chapter 3

Methodology

The proposed three-dimensional rectangular hexahedron meshing (3D RHM) single-cell model for ECIS measurement system will be discussed in this section. Three kinds of software are used to assist the modeling process – Gmsh 2.7 for mesh generation, MATLAB for impedance insertions and boundary conditions, and Synopsys HSPICE for solving 3D impedance networks. The details of modeling process are shown in Fig.12. Moreover, the strategy of mesh generation borrows the idea from finite-difference time-domain (FDTD) tensor mesh in the field of electromagnetics (EM). In this case, the mesh nodes in the interested region can be denser and finer, while the mesh nodes is set coarser in less significant area, e.g. in bulk medium region.

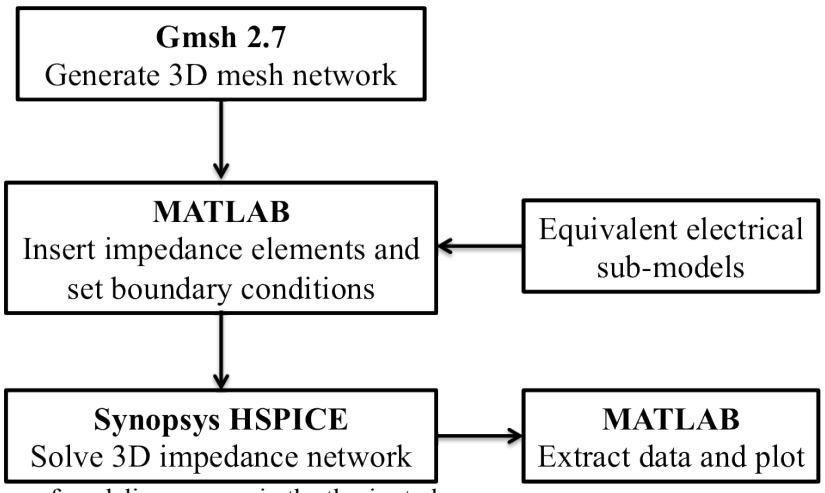

Figure 12 Overview of modeling process in the thesis study.

Since the model is totally solved numerically, the priorities of using single-cell modeling can be summarized as: 1) no commercial FEM simulator is needed; 2) the impedance component between every two mesh nodes can be derived based on different application necessities,

meaning that local sub-models can be applied to each position in 3D mesh network; 3) no approximation is needed to simplify spreading resistance, cytoplasma and distribution of current flow.

3.1 Mesh Generation

For an ECIS measurement system, we can build an environment with electrodes, electrolyte and cell. Since the hemisphere cannot be the real geometry of cell after it spreads on the electrode, the cell can be considered either a spherical cap or a cylindrical disk with diameter 30 μm and height 5 μm. Thus, the working electrode is selected in a square shape 30 μm x 30 μm. A large cuboid, 60 μm x 60 μm x 30 μm, serves as the bulk medium to construct a well for the system, where the working electrode is located at the center of bottom surface and the counter electrode is the whole surface on the top. The virtual ECIS system for single-cell model is illustrated in Fig. 13.

(A)

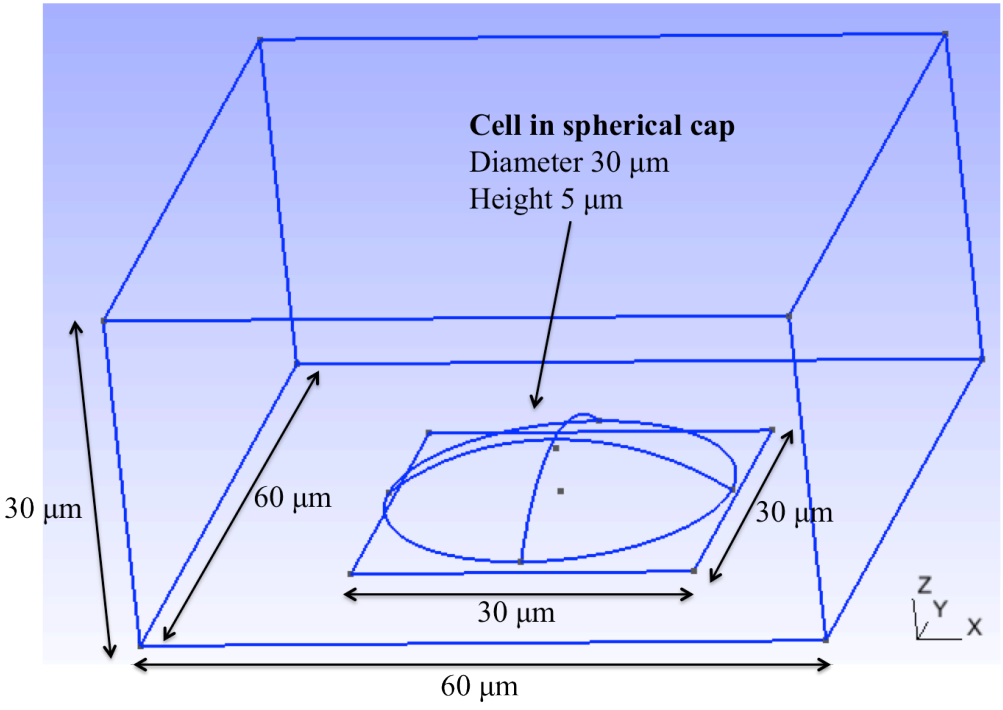

(B)

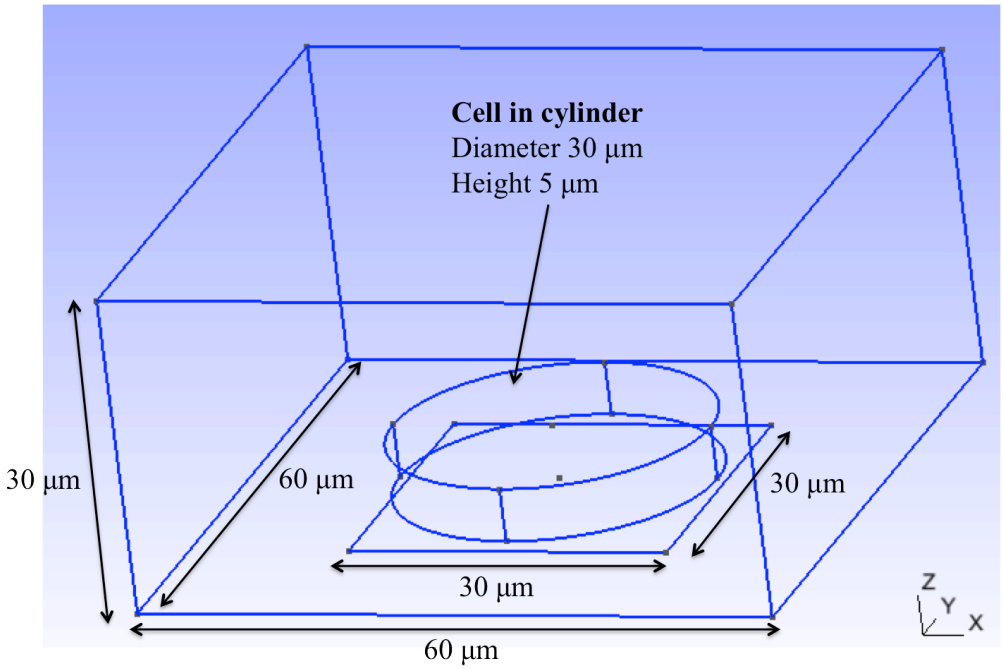

Figure 13 Illustrations of simulated ECIS measurement system for single cell, drawn by Gmsh 2.7. The smaller square at the bottom is the working electrode, while the whole top surface is the counter electrode. (A) Single cell as a spherical cap in 30 µm diameter and 5 µm height. (B) Single cell as a cylinder in 30 µm diameter and 5 µm height.

After finishing the system design, we can start to mesh the whole cuboid space. It is recommended to use Gmsh 2.7 to generate the mesh for geometry since it is an open source software and easy to be operated. For the type of mesh element, we choose rectangular hexahedron since it can be easily drawn and controlled. Similar with the application of cuboid mesh in FDTD method for EM, we mesh denser in the space with the most interest and put fewer elements in the unimportant location to save the computation time. In ECIS measurement system, only the regions with the single cell and the working electrode are significant, while the region for bulk medium is not. Therefore, we put eleven layers of denser rectangular hexahedron, 1 µm x 1 µm x 0.5 µm, from the bottom above the working electrode with the total height of 5.5 µm. Since the cell-electrode separation ranges from tens to hundreds of nanometer but less than a half

micron meter, one more 0.5 μm layer is put into this region to ensure both the height of cell and the cell-electrode separation are included in the denser mesh region.

Since only coarse mesh is necessary in medium region, we set five layers for the rest of upper space above the cell in vertical direction, which is in the height 24.5 μm, and put eight layers in the horizontal direction with a progression of 1.3. The side and bird-eye views of the final hexahedron mesh are shown in Fig. 14. The codes for mesh generation can be referred to Appendix A.

All of mesh elements with their coordinates are exported into .msh file by Gmsh 2.7, which is further converted to .txt file to be available as an input file for MATLAB. It is shown that the number of total mesh nodes is 34425 and the number of rectangular hexahedrons is 43776. Additionally, it is meaningless to finely mesh the counter electrode region, because the area of counter electrode is much larger than the working electrode and thus the impedance of electrode/medium at counter electrode is much smaller.

(A)

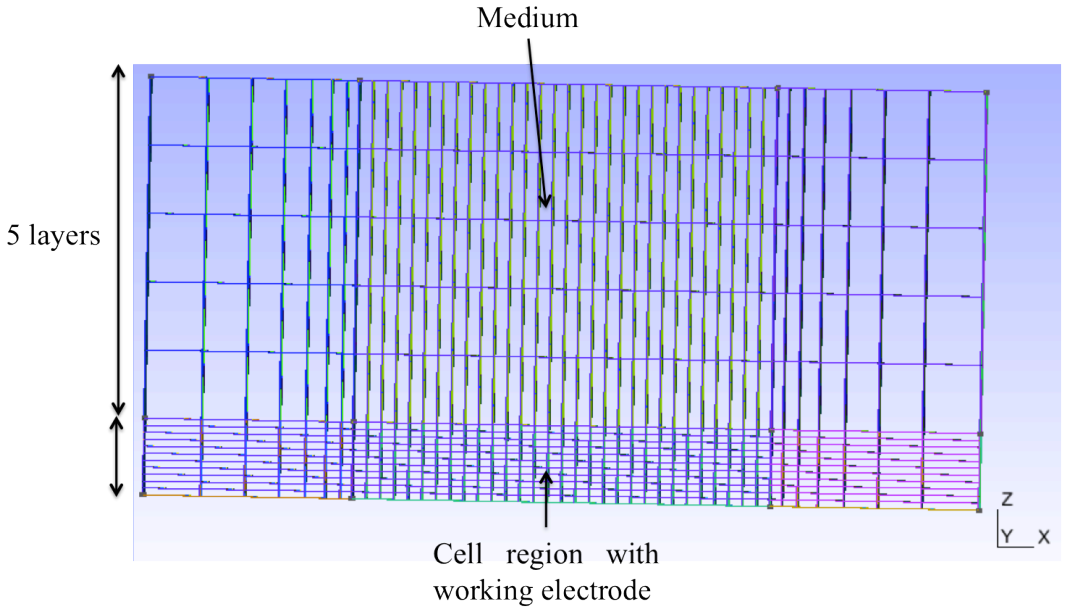

(B)

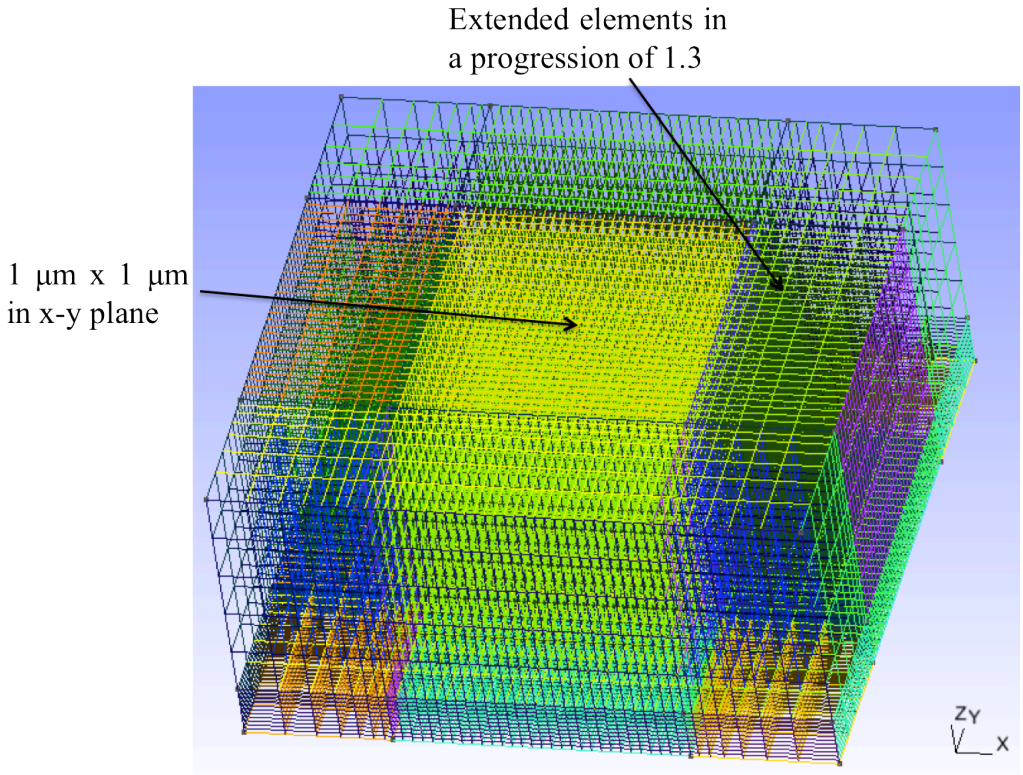

Figure 14 Generated mesh element by Gmsh 2.7. (A) Side view of rectangular hexahedron mesh. (B) Bird-eye view of rectangular hexahedron mesh. The size of mesh, 1 μm x 1 μm, keeps the same along the vertical direction in the middle space, where the working electrode is underneath. Outside the middle region, the mesh elements are extended in a progression of 1.3 to the boundaries.

3.2 Equivalent Lumped Elements and Boundary Conditions

After the .txt file containing mesh node coordinates and hexahedron elements is available, it is imported into MATLAB to establish a three-dimensional network with equivalent lumped elements. Finally, a .sp file with the information of resistors and capacitors will be outputted from MATLAB to be solved by HSPICE, which will be explained in Section 3.3.

Since a hexahedron element has 8 nodes and 12 sides, 12 electrical elements will be inserted between two nodes. In the electrical lumped element models, the values of resistance and capacitance depend on the area A and the distance L, i.e.

$$R = \frac{\rho L}{A} \tag{15}$$

$$C = \frac{\varepsilon A}{L} \tag{16}$$

where ρ is resistivity and ε is dielectric constant.

In the field of electrochemistry and biology, specific impedance is normally used to calculate the impedance of double layer and cell membrane. Thus the new equations are written as

$$R = \frac{R_{spec}}{A} \tag{17}$$

$$C = AC_{spec} \tag{18}$$

where R_{spec} and C_{spec} stand for specific resistance and capacitance, respectively.

To be specific, the 3D impedance network for single-cell model is composed of four parts: 1) the double layer at electrode/electrolyte interface; 2) cell membrane; 3) cell cytoplasm; and 4) medium surrounding the cell. As shown in Fig. 6, the double layer equivalent impedance includes a double layer capacitor C_d, a charge-transfer resistor R_{ct} and Warburg impedance, According to the Bard's derivation, Warburg impedance is calculated as:

$$Z_{W,n} = R_{W,n} + \frac{1}{j\omega C_{W,n}} \tag{19}$$

and

$$R_{W,n} = \frac{k}{A_n \omega^{1/2}} \tag{20}$$

$$C_{W,n} = \frac{A_n}{k\omega^{1/2}} \tag{21}$$

where k is a constant in Ω $sec^{-0.5}$ cm^2 and ω is the frequency equal to $2\pi f$.

Thus, we can get

$$Z_{W,n} = \frac{k}{A_n \omega^{1/2}}(1 - j) \tag{22}$$

and

$$Z_{Interface,n} = (j\omega C_d A_n + (\frac{k}{A_n \omega^{1/2}}(1-j))^{-1})^{-1} \propto A_n^{-1} \tag{23}$$

Since C_d and k can be obtained from the measurement and literatures, A_n is an important parameter which needs to be defined for two neighboring mesh nodes.

Similarly, the impedance of cell membrane is also inversely proportional to the effective area A_n between two nodes

$$Z_{Membrane,n} = \frac{1}{j\omega C_m A_n} \propto A_n^{-1} \tag{24}$$

For resistance of cytoplasm and medium (solution), both effective length L_n and area A_n are contributing, i.e.

$$R_{Cyto} = \frac{\rho_{Cyto} L_n}{A_n} \tag{25}$$

$$R_{S,n} = \frac{\rho_S L_n}{A_n} \tag{26}$$

As a result, it is important to accurately define L_n and A_n.

To define L_n is easier since it can be set as the real length between two nodes in 3D mesh. For effective area A_n, we can borrow the conception from Voronoi diagram. By definition, Voronoi diagram is the conjugate plot of Delaunay triangulation, which is an approach of meshing, and the intersection surface of two adjacent Voronoi cells is the bisection of the neighboring mesh nodes. Thus, we can consider such intersection surface as the effective area A_n. Apparently, the 3D Voronoi cell of a node from rectangular hexahedron meshing is also a rectangular hexahedron and therefore the intersection surface must be a rectangle. The illustration of Voronoi cell for rectangular hexahedron meshing is given in Fig. 15. Additionally,

it should be careful to deal with the nodes at the boundaries for the bulk cuboid in Fig. 14 when deriving the Voronoi cells since they cannot extend over the edges.

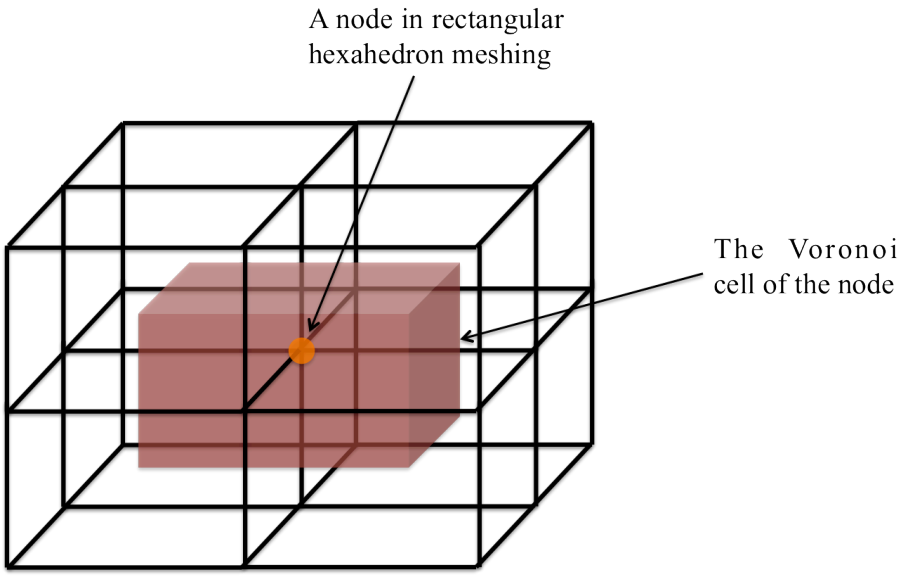

Figure 15 Voronoi cell of a node in rectangular hexahedron meshing.

After obtaining the effective area A_n and the length L_n, we can start to calculate the impedance between every two nodes. As illustrated in Fig. 16(A), the impedance can be differentiated according to the position of two neighboring nodes. The values of impedance are given in Fig. 16(B), where each impedance module may include one or more equivalent electrode lumped elements. In addition, the impedance for double layer is set separately since the interface is only around 2 nm and meshing for this area is meaningless.

The last step is to set the boundary conditions. The bottom of 60 μm x 60 μm x 30 μm bulk is applied with input sinusoidal signal V_{in} and the top is connected to ground, i.e. 0 V. The final impedance values are exported from MATLAB into a file with .sp format, which is readable for HSPICE.

(A)

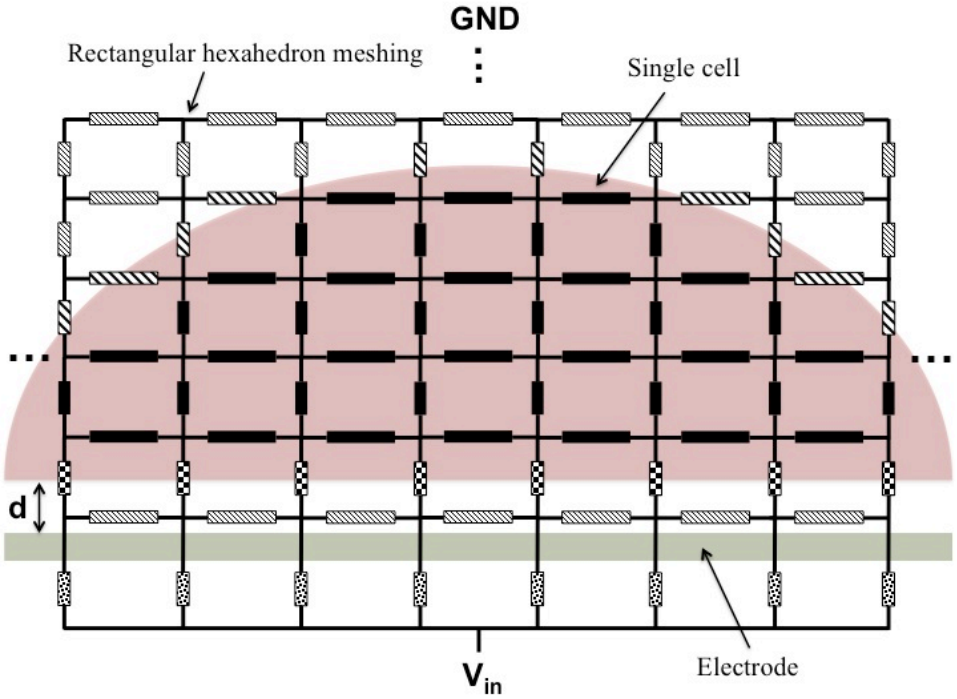

(B)

Electrode/solution interface:

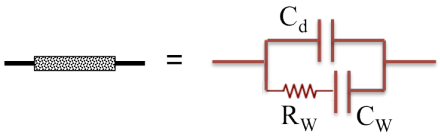

$$Z_{Interface,n} = \left(j\omega C_d A_n + \frac{A_n \omega^{1/2}}{k(1-j)}\right)^{-1}$$

Bottom cell membrane/electrode:

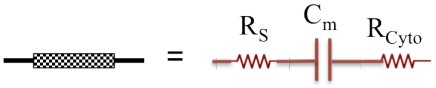

$$Z_{Bottom,n} = \frac{\rho_S d}{A_n} + \frac{1}{j\omega C_m A_n} + \frac{\rho_{Cyto}(L_n - d)}{A_n}$$

Side cell membrane/solution:

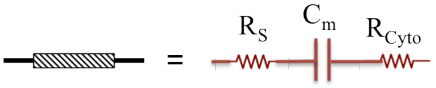

$$Z_{Side,n} = \frac{\rho_S (L_n/2)}{A_n} + \frac{1}{j\omega C_m A_n} + \frac{\rho_{Cyto}(L_n/2)}{A_n}$$

Cytoplasm:

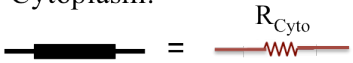

$$Z_{Cyto,n} = \frac{\rho_{Cyto} L_n}{A_n}$$

Solution:

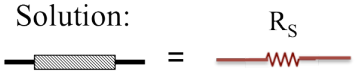

$$Z_{S,n} = \frac{\rho_S L_n}{A_n}$$

Figure 16 (A) Hexahedron meshing and corresponding inserted impedance elements. The meshing is not to scale. (B) The sub-models for each component in reconstructed ECIS system.

3.3 Three-dimensional Electrical Network Computation

HSPICE input files in .sp format are generated for each single frequency and solved by HPSICE, where the magnitude of V_{in} is set as 1V. The final results are complex currents obtained from SPICE Explorer, which reads the output files in .ac format created by HSPICE and converts it to .txt files. Finally, .txt files with the information of currents are read by MATLAB again to obtain the total impedance of the system and then plotted.

Chapter 4

Results and Discussions

First, the 3D RHM single-cell model will be used to compare with the measurement and simulation results to verify the model. Second, the model is applied to calculate the impedance with variance of cell morphology, size, cytoplasm resistivity, membrane capacitance, and cell-electrode distance, and understand the frequency-dependent cell behaviors. It will be shown that the change of total impedance due to cell properties can be mapped onto different frequency ranges in the whole spectrum from 100 Hz to 10 MHz.

4.1 Comparison with Published Measurement and Simulation Results

4.1.1 Comparison with Single Cell Measurement

In this subsection, the single-cell model will be applied to compare with the ECIS measurement data published in 2010 [5]. As shown in Fig. 10, silicon oxide was etched by 1 μm to create a circular microelectrode in 30 μm diameter. The microelectrode in 1000 Å Au layer was coated with two types of peptides, lysine-arginine-glycine-aspartic acid (KRGD) and fibronectin to improve the cell adhesion. Single fibroblast cell (NIH3T3) spread on the electrode and coverage around 95 % was observed by optical microscope. The peripheral circuits for this measurement are similar with the illustration in Fig. 1 and the final results are given as root mean square (RMS) voltage read by lock-in amplifier [5].

Since the researchers used a simple model shown in Fig, 10 with n equal to 5 to fit the measured results from 1 kHz to 10 kHz and obtained fitting parameters for electrode/medium

interface, cell membrane, cytoplasm and cell-electrode distance, the same values are applied into the single-cell model to calculate RMS voltages. The details of fitting parameters and peripheral circuits are given in Appendix B. In this case, the cell morphology is set as a hemisphere in 30 μm diameter, same as the structure modeled by Thein. In addition, the boundary condition for electrode is changed accordingly, different from the discussion in Section 3, since the circular electrode is used in this simulation. As shown in Fig. 17, the simulated results by 3D RHM single-cell model are close to the measured RMS voltages. From both simulation and measurement results, it can be seen that the RMS voltages with KRGD are larger than those with fibronectin, which indicates KRGD is more effective to improve cell adhesion.

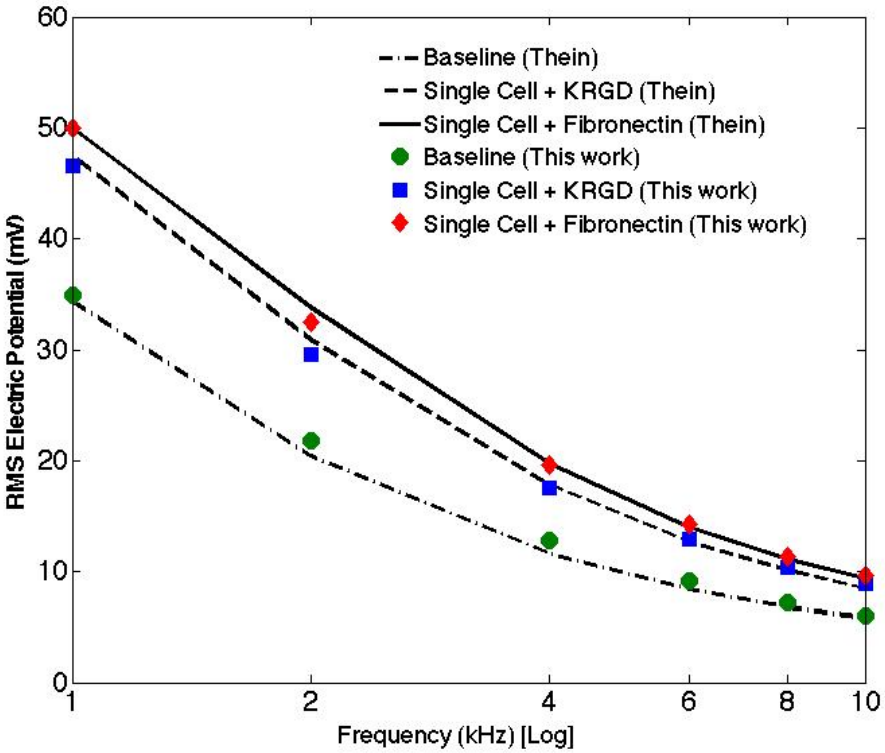

Figure 17 3D single-cell model for Au microelectrode in 30 μm diameter and NIH3T3 single cell. The RMS voltages by simulation (in dots) fit the measured results (in lines). Baseline presents the simulation and measurement without cell. Two kinds of peptides are utilized to compare the cell adhesion.

However, the simulation cannot perfectly match the measurement. The reasons may be concluded: (1) the parameters used in single-cell simulation are obtained from the data fitting by

Thein's simple model and thus the values may not be accurate, (2) the parasitic resistance and capacitance may exist in the measurement system, and (3) the single-cell model fully meshes the whole hemi-spherical cell; in contrast, Thein's model simplified the geometry of top cell membrane and cytoplasm. Even though the offsets between simulation and measurement still exist, the 3D RHM single-cell model is verified to be useful by such comparison.

4.1.2 Comparison with Single Cell FEM Modeling

Single cell modeling by COMSOL FEM approach was developed by Huang in 2004, as shown in Fig. 9 [12]. Different from Thein's model, FEM model fully considered the cell morphology and surrounding circumstances by establishing a cuboid measuring environment. In Huang's model, the working electrode is a 30 μm x 30 μm square and the cell is nicely drawn in software. In order to mesh the electrode/medium interface and cell membrane for FEM, these two regions are extended to 5 μm height. The main focus of Huang's work is to understand the distribution of current flow under different frequencies and various cell-electrode distances, which determine the sensitivity of ECIS system since more information from cell can be detected when larger percentage of current flows through the cell but not the underneath cell-electrode region.

The scanning frequency for Huang's model and 3D RHM single-cell is from 100 Hz to 10 MHz. For the consideration of uniformity, the parameters in 3D RHM model for cell/medium interface, cell membrane and medium keep the same as those in Huang's work. Moreover, the resistivity of cytoplasm is selected as 100 Ω cm to fit Huang's simulated results. In addition, the surface of working electrode is meshed by 1 μm x 1 μm small squares leading to 900 elements in total. The details of parameters are shown in Appendix C.

The computed total impedance and the normalized impedance with two different cell-electrode distances, 0.15 μm and 0.015 μm, are shown in Fig. 18.

(A)

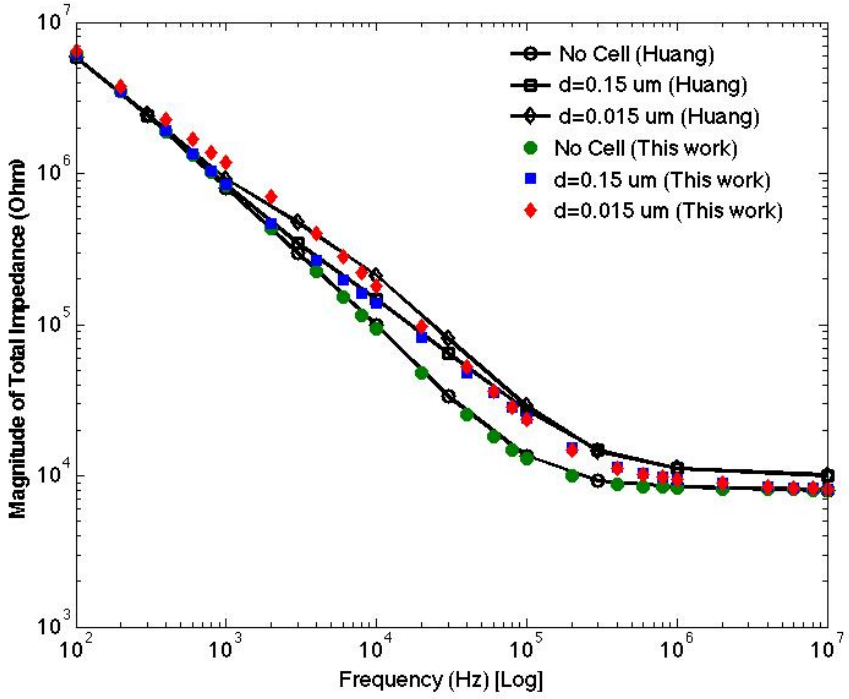

(B)

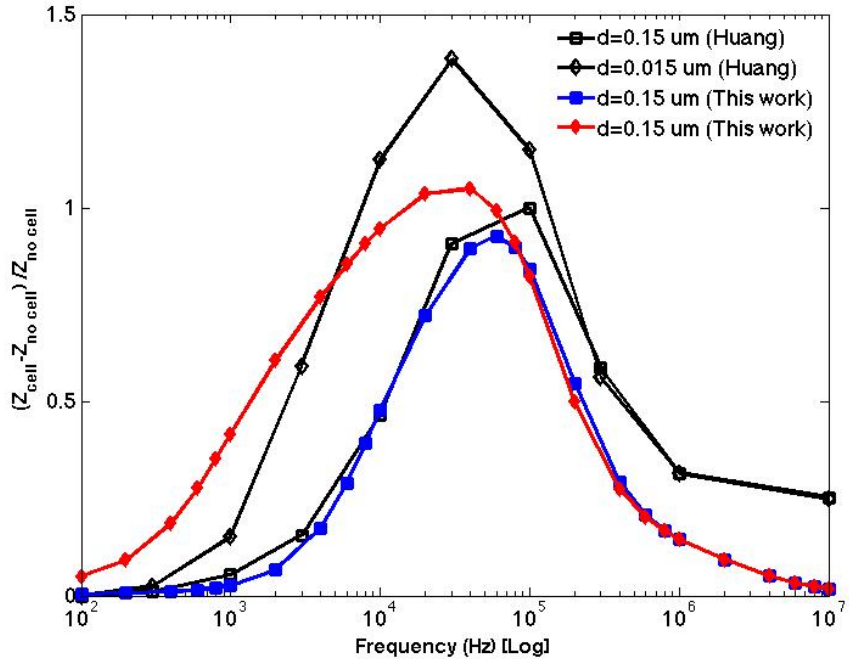

Figure 18 (A) Calculated total impedance when cell-electrode distances are 0.15 μm and 0.015 μm, respectively. (B) The normalized impedance with the same cell-electrode distances.

Compared with the simulation results from Huang's FEM modeling, the 3D RHM single-cell model shows a nice fitting to the order of impedance magnitude and frequency range of peaks for normalized impedance. The diversity of values between two models may be revealed as: (1) the thicknesses of double layer and cell membrane in Huang's FEM model are changed to satisfy the meshing necessity, (2) no internal current is considered in 3D RHM single-cell model for double layer and cell membrane due to tiny thickness, while such current exists in 0.5 μm thick regions in Huang's computation, and (3) the geometry of single cell in Huang's simulation slightly differs from the one in 3D RHM single-cell model where the spherical cap with 5 μm height is applied. Additionally, the impedance with cell at high frequency is slightly larger than the impedance without cell in Huang's simulation results, which is different from the results given by 3D RHM modeling. Since the value of cytoplasm resistivity used in Huang's simulation is not reported [12], it may be argued that a much larger number is selected compared with the one used in own single-cell model by the thesis work where the value is assumed as 100 Ω cm. When the frequency is pushed up to 10 MHz, cell membrane becomes almost transparent and cytoplasm can be considered as an extra resistor connected on the working electrode which leads the increase of final value of impedance.

The most significant information in Fig. 18 is that the change of impedance due to variance of cell-electrode distance can be observed from low frequency 100 Hz to intermediate frequency 100 kHz, where the maximum difference for normalized impedance in two distance cases is located between 1 kHz to 10 kHz. In low frequency range, the current is forced to pass through the underneath region between the bottom of cell and the electrode since the membrane acts as an insulator, and hence the change of total impedance at low frequency is largely contributed to such seal resistance. As a result, the cell adhesion that determines the cell-

electrode distance can be extracted at low operating frequency in ECIS measurement, which allows us to map the cell characteristics properly into the spectrum of frequency.

4.2 Frequency-dependent Cell Behaviors and Mapping Method

The 3D RHM single-cell model will be applied to explore the frequency-dependent cell behaviors and the sensitivity of ECIS measurement for cell properties under different operating frequencies. Four cellular characteristics are discussed in this section: size of cell (D_{cell}), cell membrane capacitance (C_m), cell-electrode distance (d), and cytoplasm resistivity (ρ_{cyto}). The first element D_{cell} is an essential parameter related to cell spreading, cytotoxicity and drug treatment for the research in the field of cancer. Membrane capacitance differs from one type of cell to another and also it may become larger when it is folded [22, 26]. Moreover, apoptosis is determined by the cell adhesion, which can be translated into the change of cell-electrode distance. Last but not least, if variance of cytoplasm resistivity can be detected by ECIS measurement, more internal cellular structure may be extracted in real-time and high-speed.

Three values of cell diameter are used in simulation: 20 μm, 25 μm and 30 μm, corresponding to three different values of height in 3.33 μm, 4.17 μm and 5 μm. The final results are plotted in normalized impedance versus frequency, since it is more straightforward to observe the change of total impedance in this approach. The meshing of the mimic ECIS system is already shown in Section 3. Additionally, the electrical model and fitting parameters for electrode/medium interface are referred to the values as Huang's model given in Appendix C.

4.2.1 Cell Behavior - Cell Membrane Capacitance (C_m)

Cell membrane capacitance varies from 1 μF/cm^2 to 5 μF/cm^2. The selection of values are referred to Giaever's model for transepithelial cells [22]. The normalized impedance for single cells in both spherical cap and cylindrical disk is shown in Fig. 19. Interestingly, the decrease of impedance can be easily observed while the membrane capacitance is increased. This is because the larger value of capacitance leads to the smaller impedance, i.e. $Z=1/j\omega C$. At low frequency, current is forced to flow through cell-electrode region since the impedance of cell membrane is large enough to block the current flow. On the other hand, the membrane impedance is small with high operating frequency and consequently current can easily pass through the cell. As a result, the peak of normalized impedance is located around 40 kHz and the maximum separation between impedance with different capacitance values starts from 10 kHz to 100 kHz. In addition, it is observed that the change of cell size can largely affect the total impedance. This can be explained that the total impedance is proportional to the coverage of cell on working electrode.

(A)

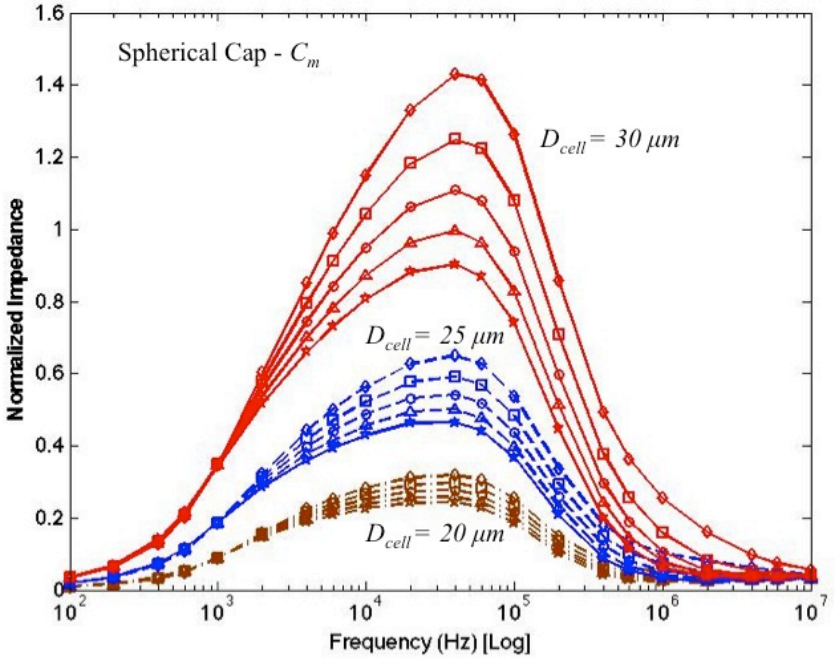

(B)

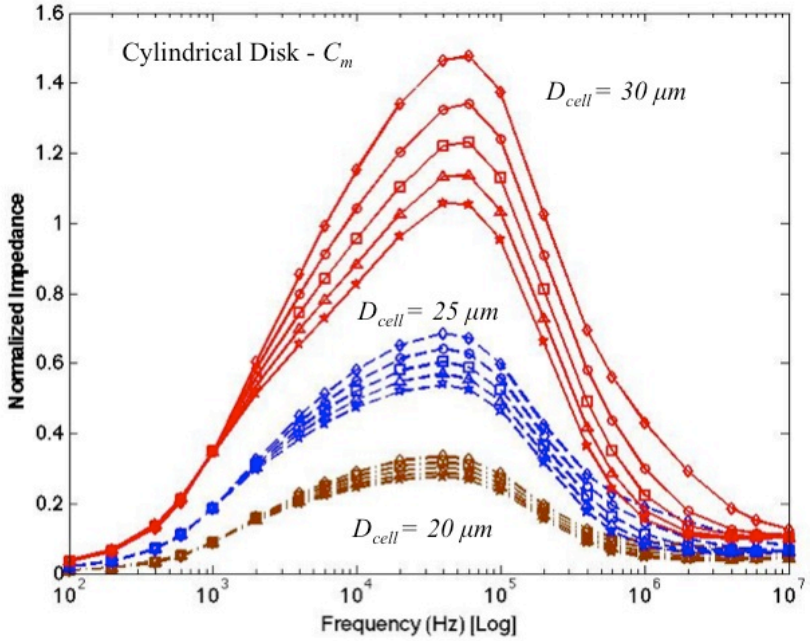

Figure 19 Normalized impedance as the function of cell membrane capacitance. (◊): C_m=1 μF/cm^2. (□): C_m=2 μF/cm^2. (O): C_m=3 μF/cm^2. (Δ): C_m=4 μF/cm^2. (★): C_m=5 μF/cm^2. The diameters of cell vary from 20 μm to 30 μm with constant size of working electrode.

4.2.2 Cell Behavior – Cell-Electrode Distance (*d*)

Five values of cell-electrode distance are selected for the simulation: 10 nm, 50 nm, 100 nm, 150 nm and 200 nm. Those numbers are compatible to calculated results from the pervious studies by Giaever and Keese [18]. The normalized impedance is shown in Fig. 20.

Different from the previous case of cell membrane capacitance, the change of total impedance is more sensitive at the frequency below 40 KHz because current prefers to flow underneath the cell instead of passing through the highly insulated membrane. In high frequency range, large percentage of current flows into the membrane and the cell-electrode distance will not affect the current path. It is also shown from Fig. 20 that the sensitivity of measurement is also depended on the values of distance: when *d* is below 100 nm, the change of total impedance due to distance variance is much larger compared with the case when d is over 100 nm. Therefore, in order to observe the variance of impedance better, microelectrode is always

modified by kinds of peptide to improve the cell adhesion and in turn reduce the cell-electrode distance.

(A)

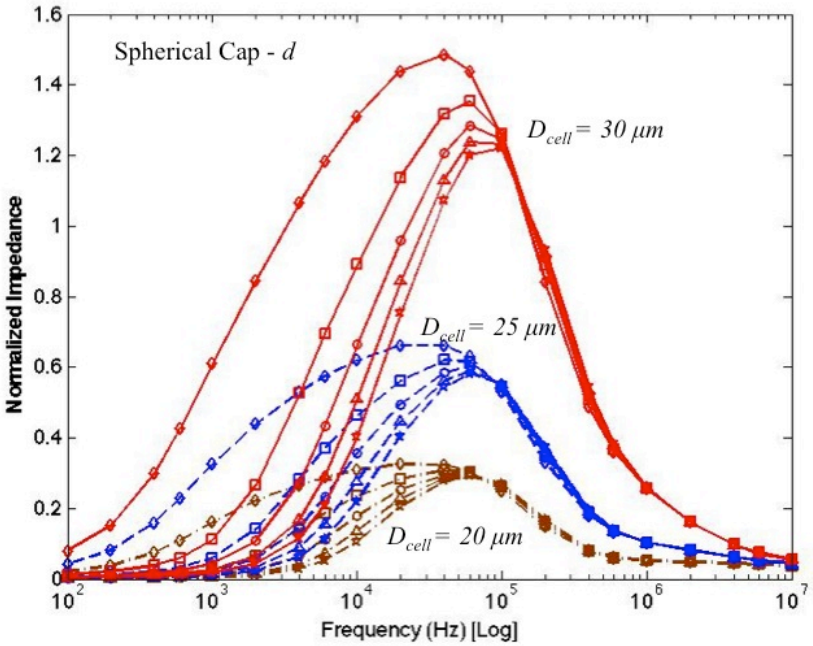

(B)

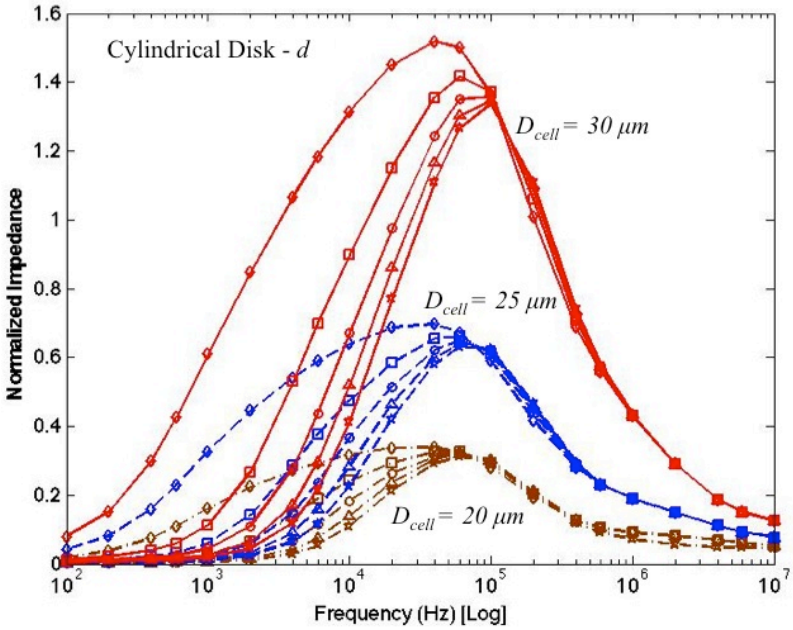

Figure 20 Normalized impedance as the function of cell-electrode distance. (◊): *d*=10 nm. (□): *d*=50 nm. (O): *d*=100 nm. (Δ): *d*=150 nm. (★): *d*=200nm. The diameters of cell vary from 20 μm to 30 μm with constant size of working electrode.

4.2.3 Cell Behavior – Cytoplasm Resistivity (ρ_{cyto})

Measurement for internal cellular structure such as cytoplasm and organelles is rarely done in the field of ECIS, especially for single cell studies. A possible reason is that the real experimental environment is mixed with many noise sources to make the measurement for intracellular information extreme difficult. Meanwhile, the design of microelectrode geometry may also be a challenge in order to observe the intracellular structures. If most of current flow can be engineered to pass through the cell itself instead of underneath the cell, the intracellular information will be projected into the measured impedance and any alternation happened inside the cell can also give the response to the change of normalized impedance. To understand the possibility of this purpose, the single-cell model is used to compute the impedance versus the change of cytoplasm resistivity ranging from 50 Ω cm to 250 Ω cm also for both cellular geometry – spherical cap and cylindrical disk. The normalized impedance versus cytoplasm resistivity is shown in Fig. 21.

(A)

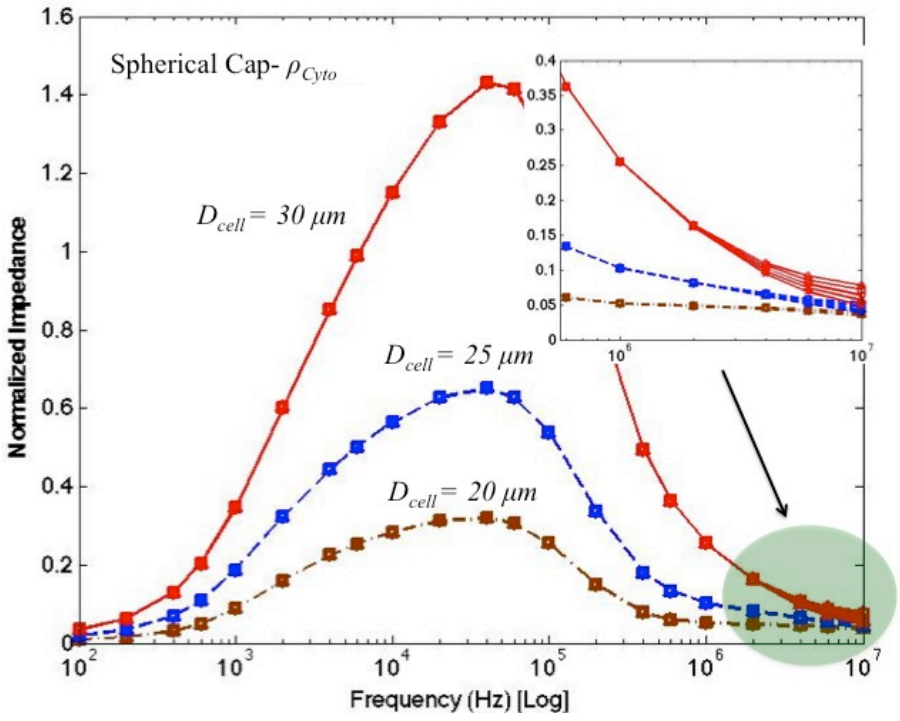

(B)

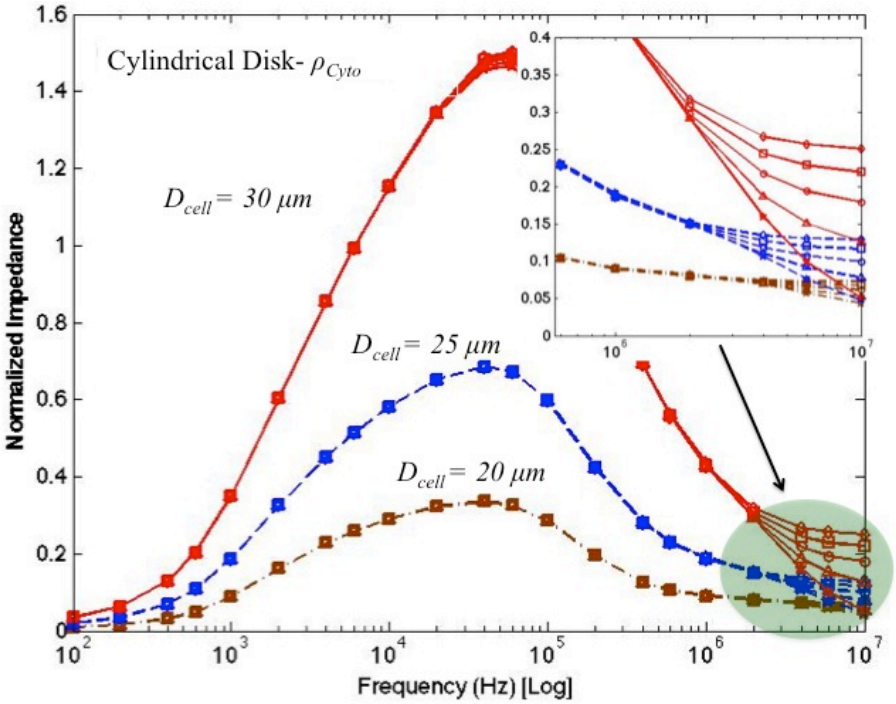

Figure 21 Normalized impedance as the function of cytoplasm resistivity. (◊): ρ_{cyto}=50 Ω cm. (□): ρ_{cyto}=100 Ω cm. (O): ρ_{cyto}=150 Ω cm. (Δ): ρ_{cyto}=200 Ω cm. (★):ρ_{cyto}=250 Ω cm. The diameters of cell vary from 20 μm to 30 μm with constant size of working electrode.

Unlike cell membrane capacitance and cell-electrode distance, the normalized impedance only tends to change at very high operating frequency in this situation. The inset in Fig. 21(B) shows more variance compared with the one in Fig. 21(A). This is because the volume of cytoplasm is larger in cylindrical cell and thus the impedance given by intracellular electrolyte can be more observable.

4.2.4 Mapping of Frequency-dependent Cell Behaviors

The projection of cellular behaviors onto frequency spectrum detected by ECIS system is summarized in Table 2.

With the constant size of cell, the change of impedance inside a certain range of frequency obtained from measurement can be used to compare with mapping table to find out the

contributing factors. When the cell spreads or shrinks, the total impedance will increase in all range of frequency spectrum. Therefore, this method is powerful because different types of cellular behaviors are now distinguishable by only one-time measurement. It is promising that the sensitivity of detection can also be improved with well-designed electrode geometry to reduce the range of 'best monitoring frequency'. In this case, 3D RHM single cell model will largely assist to compute the system impedance with different types of electrodes and various shapes of single cells in an effective and efficient way.

Table 2 MAPPING OF CELL BEHAVIORS IN FREQUENCY SPECTRUM

Cell Behavior	Cell-electrode distance	Cell membrane	Cytoplasm	Cell size
Best Monitoring Frequency (Hz)	$10^2 – 10^4$	$10^4 – 10^5$	$> 10^6$	All range

Chapter 5

Conclusion

The 3D RHM single-cell modeling method is developed to construct ECIS measurement system for detection of cellular behaviors. By computing the total impedance with different values of cell characteristics – cell geometry, cell membrane capacitance, cell-electrode distance, and cytoplasm resistivity, it is found that the change of impedance resulting from various contributing factors can be projected onto different ranges in frequency spectrum. Finally, the prototype of cellular behavior mapping is shown and can be used as a reference for further modeling and measuring studies.

Some recommendations are given for future ECIS research: (1) the rectangular hexahedron meshing can be denser and MATLAB coding should be optimized to save computation time, (2) cell morphology used for modeling should match the shape observed by optical microscope, (3) the electrical parameters for electrode/medium double layer should be firstly measured and then plugged into the model since the impedance may be not perfectly proportional to $\omega^{-1/2}$, and (4) more cellular properties should be modeled and measured to replenish the mapping table.

Bibliography

[1] I. Giaever and C. Keese, "A morphological biosensor for mammalian cells," *Nature,* vol. 366, 1993, pp. 591-592.

[2] I. Giaever and C. Keese, "Monitoring fibroblast behavior in tissue culture with an applied electric field," *Proc. Natl. Acad. Sci. USA,* vol. 81, 1984, pp. 3761-3764.

[3] Applied Biophysics. http://www.biophysics.com

[4] ACEA Biosciences. http://www.aceabio.com/main.aspx

[5] M. Thein, F. Asphahani, A. Cheng, R. Buckmasterm, M. Zhang, and J. Xu, "Response characteristics of single-cell impedance sensors employed with surface-modified microelectrodes," *Biosens. Bioelectron.,* vol. 25, 2010, pp. 1963-1969.

[6] C. Xiao and J. Luong, "A simple mathematical model for electric cell-substrate impedance sensing with extended applications," *Biosens. Bioelectron.,* vol. 25, 2010, pp. 1774-1780.

[7] A. Guyton and J. Hall, Textbook of Medical Physiology, 11th ed. Pennsylvania: Elsevier Inc., 2006, ch.2.

[8] I. Giaever and C. Keese, "Use of electric fields to monitor the dynamical aspect of cell behavior in tissue culture," *IEEE T. Bio-Med Eng.,* vol. 33, 1986, pp. 242-247.

[9] J. Atienza, J. Zhu, X. Wang, X. Xu, and Y. Abassi, "Dynamic monitoring of cell adhesion and spreading on microelectronic sensor arrays," *J. Biomol. Screen.,* vol. 10, 2005, pp. 795-805.

[10] Y. Qiu, R. Liao, and X. Zhang, "Impedance-based monitoring of ongoing

cardiomyocyte death induced by tumor necrosis factor-α," *Biophys. J.,* vol. 96, 2009, pp. 1985-1991.

[11] F. Asphahanim, K. Wang, M. Thein, O. Veiseh, S. Yung, J. Xu, and M. Zhang, "Single-cell bioelectrical impedance platform for monitoring cellular response to drug treatment," *Phys. Biol.* vol. 8, 2011, 015006.

[12] X. Huang, D. Nguyen, D. Greve, and M. Domach, " Simulation of microelectrode impedance changes due to cell growth," *IEEE Sens. J.,* vol. 4, 2004, pp. 576-583.

[13] A. Bard and L. Faulkner, *Electrochemical Methods: Fundamentals and Applications*, 2nd ed. New York: John Wiley & Sons, Inc., 2001, ch.1, 10.

[14] W. Franks, I. Schenker, P. Schmutz, and A. Hierlemann, "Impedance characterization and modeling of electrodes for biomedical applications," *IEEE T. Bio-Med Eng.,* vol. 52, 2005, pp. 1295-1302.

[15] S. Grimnes and Ø. Martinsen, *Bioimpedance & Bioelectricity Basics*, 2nd ed. Oxford: Elsevier, Inc., 2008, ch.5.

[16] M. Stelzle and E. Sackmann, "Sensitive detection of protein adsorption to supported lipid bilayers by frequency-dependent capacitance measurements and microelectrophoresis," *BBA.,* vol. 981, 1989, pp. 135-142.

[17] Y. Kanno and W. Loewenstein, "A study of the nucleus and cell membranes of oocytes with an intra-cellular electrode," *Exp. Cell. Res.,* vol. 981, 1963, pp. 149-166.

[18] I. Giaever and C. Keese, "Micromotion of mammalian cells measured electrically," *Proc. Natl. Acad. Sci. USA,* vol. 88, 1991, pp. 7896-7900.

[19] T. Gowrishankar and J. Weaver, "An approach to electrical modeling of single and multiple cells," *Proc. Natl. Acad. Sci. USA,* vol. 100, 2003, pp. 3203-3208.

[20] D. Stewart, T. Gowrishankar and J. Weaver, "Transport lattice approach to describing cell electroporation: use of a local asymptotic model," *IEEE T. Plasma Sci.,* vol. 32, 2004, pp. 1696-1708.

[21] T. Gowrishankar, K. Smith and J. Weaver, "Transport-based biophysical system models of cells for quantitatively describing responses to electric fields," *P. IEEE,* vol. 101, 2013, pp. 505-517.

[22] C. Lo, C. Keese, and I. Giaever, "Impedance analysis of MDCK cells measured by electric cell-substrate impedance sensing," *Biophys. J.,* vol. 69, 1995, pp. 2800-2807.

[23] X. Huang, D. Greve, D. Nguyen, and M. Domach, "Impedance based biosensor array for monitoring mammalian cell behavior," *P. IEEE Sensors,* vol. 1, 2003, pp. 304-309.

[24] F. Asphahani, M. Thein, O. Veiseh, D. Edmondson, R. Kosai, M. Veiseh, J. Xu, and M. Zhang, "Influence of cell adhesion and spreading on impedance characteristics of cell-based sensors," *Biosens. Bioelectron.,* vol. 23, 2008, pp. 1307-1313.

[25] F. Asphahani, K. Wang, M. Thein, O. Veiseh, S. Yung, J. Xu, and M. Zhang, "Single-cell bioelectrical impedance platform for monitoring cellular response to drug treatment," *Phys. Biol.,* vol. 8, 2011, 015006.

[26] L. Gentet, G. Stuart, and J. Clements, "Direct measurement of specific membrane capacitance in neurons," *Biophys. J.,* vol. 79, 2000, pp. 314-320.

Appendix A – Gmsh 2.7 Code

```
/*********************************************************************
 *
 *  Mesh (Cell)
 *
 *********************************************************************/


D = 30;
L_Bulk = 60;


// Draw the boundary
Point(1) = {-D/2, -D/2, 0};
Point(2) = {D/2, -D/2, 0};
Point(3) = {D/2, D/2, 0};
Point(4) = {-D/2, D/2, 0};


Point(5)  = {-L_Bulk/2, -L_Bulk/2, 0};
Point(6)  = {-D/2, -L_Bulk/2, 0};
Point(7)  = {D/2, -L_Bulk/2, 0};
Point(8)  = {L_Bulk/2, -L_Bulk/2, 0};
Point(9)  = {L_Bulk/2, -D/2, 0};


Point(10) = {L_Bulk/2, D/2, 0};
```

```
Point(11) = {L_Bulk/2, L_Bulk/2, 0};
Point(12) = {D/2, L_Bulk/2, 0};
Point(13) = {-D/2, L_Bulk/2, 0};
Point(14) = {-L_Bulk/2, L_Bulk/2, 0};
Point(15) = {-L_Bulk/2, D/2, 0};
Point(16) = {-L_Bulk/2, -D/2, 0};

Line(1) = {1, 2}; Line(2) = {2, 3}; Line(3) = {3, 4}; Line(4) = {4, 1};
Line(5) = {5, 6}; Line(6) = {6, 7}; Line(7) = {7, 8}; Line(8) = {8, 9};
Line(9) = {9, 10}; Line(10) = {10, 11}; Line(11) = {11, 12}; Line(12) = {12, 13};
Line(13) = {13, 14}; Line(14) = {14, 15}; Line(15) = {15, 16}; Line(16) = {16, 5};
Line(17) = {1, 6}; Line(18) = {2, 7}; Line(19) = {2, 9}; Line(20) = {3, 10};
Line(21) = {3, 12}; Line(22) = {4, 13}; Line(23) = {4, 15}; Line(24) = {1, 16};

Line Loop(1) = {1, 2, 3, 4};      Line Loop(2) = {5, -17, 24, 16};
Line Loop(3) = {6, -18, -1, 17};  Line Loop(4) = {7, 8, -19, 18};
Line Loop(5) = {9, -20, -2, 19};  Line Loop(6) = {10, 11, -21, 20};
Line Loop(7) = {12, -22, -3, 21}; Line Loop(8) = {13, 14, -23, 22};
Line Loop(9) = {15, -24, -4, 23};

Plane Surface(1) = {1}; Plane Surface(2) = {2};
Plane Surface(3) = {3}; Plane Surface(4) = {4};
Plane Surface(5) = {5}; Plane Surface(6) = {6};
```

Plane Surface(7) = {7}; Plane Surface(8) = {8};

Plane Surface(9) = {9};

Transfinite Line {1, 2, 3, 4} = 31;

Transfinite Line {6, 9, 12, 15} = 31;

Transfinite Line {17, 18, 19, 20, 21, 22, 23, 24} = 8 Using Progression 1.3;

Transfinite Line {-5, 7, -8, 10, -11, 13, -14, 16} = 8 Using Progression 1.3;

Transfinite Surface {1, 2, 3, 4, 5, 6, 7, 8, 9};

Recombine Surface {1, 2, 3, 4, 5, 6, 7, 8, 9};

Extrude {0, 0, 5.5} {Surface{1, 2, 3, 4, 5, 6, 7, 8, 9}; Layers {11}; Recombine;}

Extrude {0, 0, 24.5} {Surface{46, 68, 90, 112, 134, 156, 178, 200, 222}; Layers {5}; Recombine;}

Appendix B – Parameters in Thein's Model

Model Parameters	**KRGD-modified**	**Fibronectin-modified**
Charge transfer resistivity of surface-modified microelectrode (ρ_e) [kΩ cm^2] μΩ	10.97	11.83
Specific CPE of surface-modified microeletrode (c_{CPE}) [μF/cm^2]	186.4	195.8
CPE phase coefficient (β)	0.867	0.914
Specific cell membrane capaciance (C_m) [μF/cm^2]	97.9	83.7
Cell membrane resistivity (ρ_m) [kΩ cm^2]	0.0312	0.0286
Resistivity of cytoplasm (ρ_{Cyto}) [kΩ cm]	0.606	0.679
Cell-electrode distance (d) [nm]	14.52	11.59
Current limiting resistor (R_{limit}) [Ω]	10^6	
Input impedance for lock-in amplifier	82 pF capacitor in series with 100 kΩ resistor	

Appendix C – Parameters in Huang's Model

Model Parameters	**Values**
Parameter for Warburg impedance (k) [Ω cm^2]	5220
Specific cell membrane capacitance (C_m) [μF/cm^2]	1
Medium conductivity (ρ_s^{-1}) [Ω^{-1} cm^{-1}]	0.015